Development of Magnetic Coupling with Variable Thrust Structure for Flywheel Energy Storage System in Long Lifetime UPS

*Daisuke Sato, *Jun-ichi Itoh, *Tomoki Watanabe, *Kazuma Kawagoe, *Noboru Yamada, and **Koji Kato
*Nagaoka University of Technology
Nagaoka, Niigata, Japan
dsato@stn.nagaokaut.ac.jp, itoh@vos.nagaokaut.ac.jp
**Sanken Electric Co., Ltd.
Kawagoe, Saitama, Japan
k.kato@sanken-ele.co.jp

***Abstract*— This paper introduces the flywheel energy storage system (FESS) in a long lifetime uninterruptible power supply. The first prototype FESS (3.0-MJ) uses low cost ball bearings and general purpose induction motor in terms of cost reduction. From the experimental results, it is confirmed that the charge and discharge efficiency of the FESS is 60.7% (charge 80.7%, discharge 75.1%). In order to improve the efficiency and lifetime, a permanent magnet synchronous motor, a spherical spiral groove bearing and a magnetic coupling with variable thrust structure are applied to the second prototype. The estimated charging efficiency is achieved to 86.9% and the estimated discharging efficiency is achieved to 82.8% at the second prototype. Then, the thrust of the proposed magnetic coupling is analyzed by the finite element method (FEM). As a result, the thrust can be changed by 11.1% with the electromagnet. In addition, the thrust analysis results are evaluated by using the prototype electromagnet.**

Keywords—Energy storage; Flywheel; Magnet coupling; Thrust control

I. INTRODUCTION

An uninterruptible power supply (UPS) is widely used in order to prevent instantaneous power failure in data centers or factories. The UPS needs the energy buffer such as electric double layer capacitors (EDLCs), batteries, or flywheels because the UPS has to supply the power to load until an emergency generator starts.

Table I shows the characteristics of each energy storage devices. The battery can achieve a high energy density at low cost. However, one of the problems in the battery energy storage is the short life time. In particular, the lifetime depends on the ambient and the number of charge and discharge time. In addition, the battery cannot cope with rapid charge and discharge due to the large internal resistance in the battery. On the other hand, an EDLC has a high charge and discharge efficiency. Moreover, the rapid charge and discharge are possible because the internal resistance is very small. However, similar to the battery, the lifetime is decreased rapidly due to the influence of the ambient temperature [1]. On the other hand, flywheel energy storage systems (FESS) has following advantages compared to chemical batteries: (i) environmental friendly, (ii) low maintenance cost, (iii) long lifetime due to no chemical structure, and (iv) the charge and discharge characteristic of high cycle are excellent. For these reason, the flywheel has attracted attention as an energy storage system [2-8].

TABLE I. CHARACTERISTICS OF EACH STORAGE DEVICES.

	Flywheel	EDLC	Battery
Energy storage	Kinetic energy	Ion transfer	Chemical reaction
Charge & Discharge of short period	Fast	Fast	Slow
Temperature characteristic	Excellent	Limited by temperature	Limited by temperature
Energy density	Good	Good	Excellent

In recent years, an ultra-high speed rotation of the flywheel has been studied [2-4]. The kinetic energy which is stored in the flywheel is proportional to the square of the rotational speed. Therefore, the magnetic bearings have been studied in order to achieve high energy density. However, the conventional five-axis magnetic bearing system requires an additional control system [7]. In addition, the flexibility of this system is low because this system is necessary to design in accordance with the capacity of the power source to be compensated. On the other hand, in order to increase storage energy, it is necessary to increase the mass of the flywheel in the low speed rotation FESS because the kinetic energy is proportional to the inertia. However, when the typical ball bearing is applied, the bearing loss is increased by increasing the mass of the flywheel. Therefore, it is effective to apply spherical spiral groove bearing (SSGB) as the bearing loss reduction method for the flywheel because the SSGB can float. Furthermore, the SSGB has longer lifetime than that of the ball bearing [9].

In addition, a motor/generator for driving the flywheel is put inside the vacuum case (MG-inside type) or outside it (MG-outside type). MG-outside type has advantage in terms of heat dissipation. In addition, torque is transmitted to the flywheel by a magnetic coupling [10-11]. However, it is difficult to apply the SSGB to MG-outside type because the shaft of the SSGB side must be float, whereas the shaft of the

MG side is fixed. Therefore, the thrust of the flywheel is controlled by the proposed magnetic coupling. The proposed magnetic coupling can not only transmit torque but also control the thrust of the SSGB as the magnetic bearing. The conventional magnetic bearing has five electromagnets (two for x-axis, two for y-axis and one for z-axis). By contrast, the proposed magnetic bearing has only one electromagnet for z-axis.

In this paper, the first prototype FESS made from the general products is developed. Next, the charging and discharging efficiency are measured. Then, in order to improve the efficiency and lifetime, the PMSM, the SSGB and the proposed magnetic coupling are employed in the second prototype FESS. This paper considers the proposed magnetic coupling with variable thrust structure as the first step in order to apply the SSGB. Therefore, the thrust and the torque of the proposed magnetic coupling are analyzed by the finite element method (FEM). Besides, the prototype electromagnet is developed, and the thrust analysis results by the FEM are compared with the experimental results.

II. Construction of Flywheel Energy Storage System

Fig. 1 shows the configuration of the first prototype FESS that employs a general induction motor and ball bearings. In this system, it is possible to store the kinetic energy of 3.0 MJ at 2900 r/min. The typical ball bearing and the general purpose motor can be applied in such low rotation speed region. In addition, the flywheel vacuum case and the motor are separated by the magnetic coupling. As a result, the windage loss can be greatly reduced because it is possible to reduce the pressure in a vacuum case by the vacuum pump. Moreover, the vacuum in the vacuum case does not affect the heat dissipation of the motor because the motor and the vacuum case are separated. Therefore, the general purpose motor can be applied to drive the flywheel without adding special cooling mechanism.

Fig. 2 shows the block diagram of the flywheel system including the measurement system and auxiliary devices. In the flywheel system, the induction motor is operated as a generator during deceleration; the kinetic energy is converted into the electrical energy. On the other hand, during acceleration, the electrical energy is stored as the kinetic energy. Therefore, this system uses a regenerative converter. Furthermore, an over-temperature of the bearing and the motor can be prevented by the oil cooler.

Table II shows the specification of the flywheel. It can be seen that the shape of the flywheel is disk-shaped. The flywheel is capable of storing sufficient energy for low rotational speed due to the large inertia weight. In addition, the windage loss and the bearing losses are also reduced by the reduction of the rotational speed. The pressure in the vacuum case is reduced by using the vacuum pump in order to reduce the windage loss. In addition, the magnetic coupling is adopted to maintain the vacuum in the vacuum case.

III. Evaluation of Charge and Discharge Efficiency

In this section, the energy storage efficiency of the prototype system (Fig. 1) is analyzed. This property is divided into charging efficiency and discharging efficiency. The charging efficiency is the ratio of the energy consumed for storing the desired energy. On the other hand, the discharging efficiency is the ratio of the actual energy can be released with respect to the stored energy.

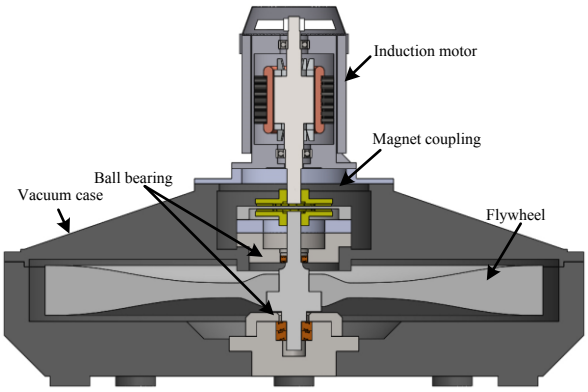

Fig. 1. Configuration of a flywheel system that employs an induction motor and ball bearings. This system can store the kinetic energy of the 3.0 MJ at 2900 r/min.

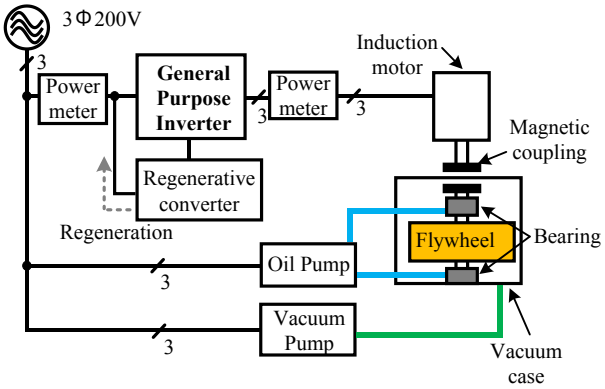

Fig. 2. Block diagram of the flywheel system including the measurement system and the auxiliary devices.

TABLE II. Specifications of the Flywheel which is Calculated from the Low Loss Design.

Flywheel	Material	SCM440
	Radius	500 mm
	Thickness	65 mm
	Weight of the Flywheel	392 kg
	Stored Energy	3.0 MJ at 2900 r/min
Motor/Generator	MLC1115C (Fuji Electric)	
Inverter	FRN 37G11S-2 (Fuji Electric)	

Fig. 3 shows the experimental results of (a) the energy storage and (b) the energy discharge. In the experiment of energy storage, the flywheel is accelerated from 2300 r/min to 2900 r/min. In the discharge test, the flywheel is decelerated from 2900 r/min to 2300 r/min. The stored energy is calculated using (1) from the rotational angular velocity and the moment of inertia of the flywheel J.

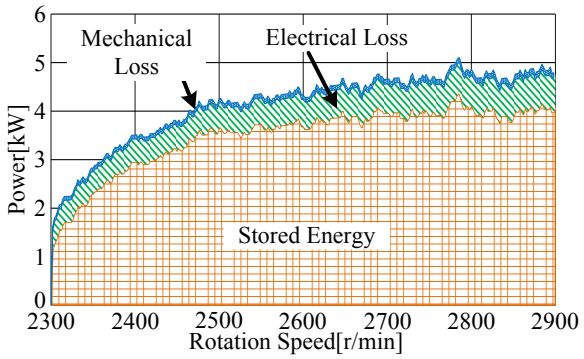

(a) Charging efficiency

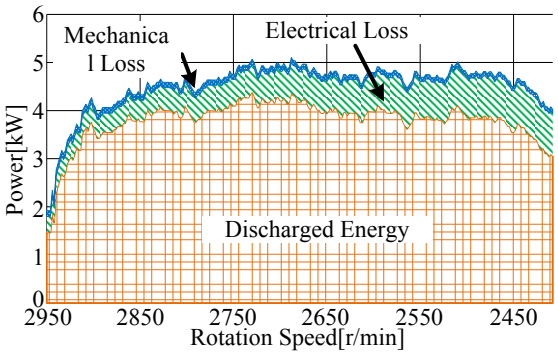

(b) Discharging efficiency

Fig. 3. Measurement results of the charging and discharging efficiency. The achieved charging efficiency is 80.7 % and the achieved discharging efficiency is 75.1 %. Therefore, the total achieved efficiency is 60.7 %.

$$E = \frac{1}{2} J\omega^2 \tag{1}$$

From (1), it is calculated that the amount of the energy change is 1 MJ when the rotational speed changes from 2300 r/min to 2900 r/min. Next, the energy storage efficiency is calculated using the experimental results. Note that, the charging efficiency is the ratio of the input energy to the stored energy. On the other hand, the discharging efficiency is the ratio of the decreasing of the kinetic energy to the regenerative energy. If only the mechanical loss is considered, it is confirmed that the achieved charging efficiency is 97.9% and the achieved discharging efficiency is 97.5%. Therefore, the total achieved efficiency is 95.2%. On the other hand, if the motor loss is considered, the achieved charging efficiency is 80.7% and the achieved discharging efficiency is 75.1%. Therefore, the total achieved efficiency is 60.7%.

Besides, the discharging efficiency of the energy storage devices is as follows: the lead acid battery is 75-85%, a redox flow battery is approximately 70%, and an EDLC is approximately 90%. Therefore, it is confirmed that the energy storage efficiency of the prototype FESS is about as same as the lead acid battery or the redox flow battery. However, the efficiency of the FESS is lower than that of the EDLC.

IV. Efficiency Improvement of FESS

The low efficiency of the first prototype FESS is caused mainly by the additional loss when the induction motor is used to drive the flywheel. Besides, the cause of the mechanical loss is the bearing loss. Thus, it is necessary to apply a PMSM and a SSGB to achieve high efficiency for the entire flywheel system. In addition, SSGB is longer lifetime than the ball bearing. However, the shaft of the SSGB side must be float, whereas the shaft of the motor side is fixed. In other words, the shaft of the SSGB needs a degree of freedom. In order to solve this problem, a magnetic coupling with a variable thrust structure is proposed in this paper. The conventional magnetic coupling is effective method to transmit torque in the isolated system such as the first prototype FESS. The proposed magnetic coupling can not only transmit torque from the motor in the atmosphere to the flywheel in vacuum but also control the thrust of the SSGB. The proposed magnetic coupling can give a degree of freedom indirectly to the SSGB.

Fig. 4 shows the configuration of the second proposed FESS in which the system of Fig. 1 is modified in order to reduce the motor loss and the bearing loss. The PMSM employs the general product due to low production cost. The ratio output of the motor is 3.7 kW. The SSGB is attached to the bottom of the flywheel.

Fig. 5 shows the analysis result of the steady state loss. The steady state loss of the first prototype is divided based on the measurement result. That of the second prototype is estimated. The rotational speed is 2900 r/min and the pressure in the vacuum case is kept at 20 Pa. The mechanical loss and the electrical loss are separated by a free-run test at the beginning. The free-run test is a test for electrically disconnecting the inverter and the motor with the stored energy in the flywheel. In this state, the stored energy is consumed only by mechanical loss. Therefore, the mechanical loss is calculated from the time until the stored energy is consumed. The motor loss of the second prototype is conjectured by the representative value. From the total loss of the first prototype is 436 W. On the other hand, that of the second prototype is 274 W. The motor loss of the second prototype is 30.4% lower than that of the first prototype, and the bearing loss of the second prototype is 88.0% lower than that of the first prototype. In addition, the loss of the magnetic coupling increases slightly by the coil current of the electromagnet. As a result, it is comfirmed that the second prototype achieves low loss as compared with the first prototype. Moreover, the estimated charging efficiency is achieved to 86.9% and the estimated discharging efficiency is achieved to 82.8% at the second prototype. Thus, it is expected to improve the charge and discharge efficiency by applying the PMSM and the SSGB.

V. Design of Magnetic Coupling with Variable Thrust Structure

In this section, the magnetic coupling with variable thrust structure is considered. The required performances of the magnetic coupling are as follows:

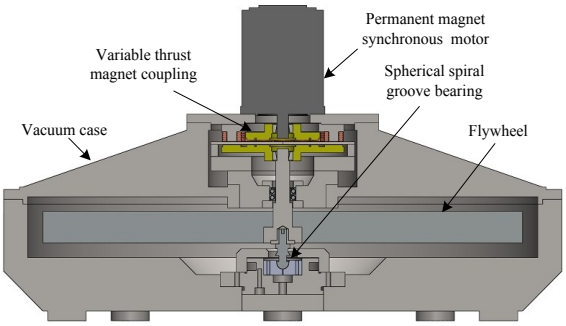

Fig. 4. Configuration of the proposed flywheel system that comprises the PMSM, the SSGB, and the proposed magnetic coupling in which the system of Fig. 1 is improved.

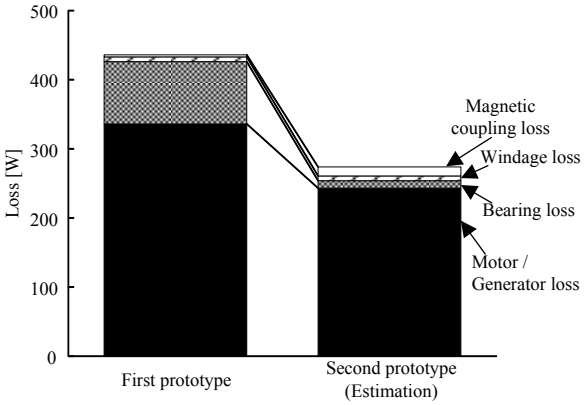

Fig. 5 Loss analysis results at the rated energy storage. The steady rotation speed is 2900 r/min and the pressure of the vacuum case is 20 Pa.

- The allowable torque is over than the maximum output torque of the PMSM (7.4 Nm).
- When the variable thrust structure does not operate, the thrust is same as the gravity of the flywheel (490 N).
- When the variable thrust structure operates, the maximum variation of the thrust is approximately 20%.

Fig. 6 shows the designed magnetic coupling with the variable thrust structure. Table III shows the parameter of the magnetic coupling. Note that the model of the electromagnets and the master side are a half model and the one of the slave side is a full model. The magnets for the torque transmission are 16 poles. The magnets in the innermost layer reduce excessive thrust by the magnets for the torque transmission. The variable thrust structure consists of the electromagnets and the outside magnet in the slave side. Note that the coil current is same in the all electromagnets. Therefore, the 16 electromagnets are operated as one large electromagnet. The current in the electromagnets generates the magnetomotive force (MMF) F. The MMF is obtained by (2).

$$F = NI \qquad (2),$$

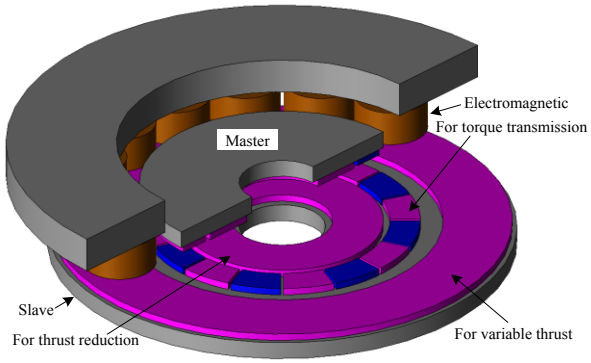

Fig. 6. Designed magnetic coupling with a variable thrust structure. Note that the model of the electromagnets and the master side are a half model and the one of the slave side is a full model.

TABLE III. PARAMETERS OF MAGNETIC COUPLING.

Pole number		16
Coil number		16
Turn number of coil		40
Rated coil current		10 A
Yoke and core		S45C
Magnet		N45M
Outer diameter	Master	155 mm
	Slave	255 mm
Inner diameter		45 mm
Thickness of magnet		4 mm
Air-gap length	Between master and slave	10 mm
	Between coil and slave	7 mm

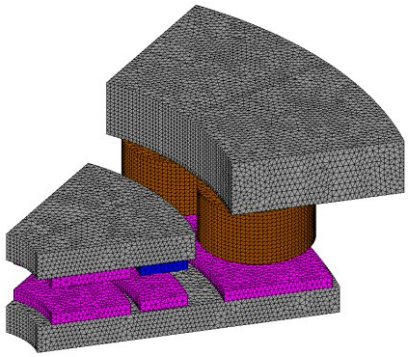

Fig. 7. Analysis model of the magnet coupling. The element count is 212,691 exclusive of the air region.

where N is the turn number of the coil and I is the current. From (2), it is understood that the MMF can be controlled by the current. In addition, the current is controlled by the inverter in order to change the MMF direction. Therefore, the thrust can be controlled indirectly by the current. Then, the thrust characteristic of the designed magnetic coupling is analyzed by the finite element method.

Fig. 7 shows the analysis model of the proposed magnet coupling. It is 45 degrees model because the coupling has

rotational symmetries. The element count is 212,691 exclusive of the air region. In addition, the upper side of purple magnets is N pole and the upper side of blue ones is S pole. The magnet temperature is 20 degree Celsius. The current polarity is defined as positive when the current flows through the coils in a counterclockwise direction. Therefore, the upward MMF (z-axis direction) polarity is defined as positive when the current polarity is positive. In this analysis, the thrust and the torque are calculated at each rotation angle when the slave side is fixed and the master side is rotated.

Fig. 8 shows the analysis result of the thrust and the torque when the variable thrust structure does not operate. From Fig. 8(a), the thrust is almost same as the design value (487 N) when the rotation angle is 0 degree and F = 0A. In addition, the slave side decreases the thrust by 11.1% when the MMF changes from 0A to -400 A. This is caused by the repulsion force between the coils ant the magnet for the variable thrust. In addition, the repulsion force is always constant with the rotation angle because the magnet for the variable thrust is one pole. From Fig. 8(b), the maximum torque is 16.7 Nm at 11.25 degree. Therefore, the allowable torque of the proposed magnetic coupling is twice maximum output torque of the PMSM. In addition, the torque at F = 0 A is same as that at F = -400 A because the direction of the MMF by the electromagnet is axial direction.

Fig. 9 shows the characteristic between thrust and MMF when the rotation angle is 0 degree. The thrust at F = 0 A is almost same as the gravity of the flywheel (487 N). The change in the thrust is 111 N between F = -400 A and F = 400 A. Therefore, the magnetic coupling can be designed as required. In addition, the thrust varies linearly with the MMF. This means that the thrust is controlled easily by the current.

VI. Evaluation of Thrust Analysis

In this section, the prototype electromagnet is developed. Then, in order to apply the thrust control by the magnetic coupling into the proposed FESS, the thrust analysis result of the electromagnet is evaluated in the experiment.

Fig. 10 shows the 2D analysis model of the prototype electromagnet. It is built by the EI-core (PC40EI60/TDK). The coil is placed in the E-core side. The turn number of coil is 140. In addition, the element count is 5,898 which include the air region. Next, the thrust of the I-core side is analyzed and measured when the MMF and the air-gap length are changed.

Fig. 11 shows the characteristic between thrust of the I-core side and MMF. The air-gap length is kept constant at 4.8 mm. From Fig. 11, the analysis result is almost same as the experimental result. In addition, the thrust is proportional to the square of the MMF. When the magnetic resistance is constant, the flux is the proportional to the MMF. Therefore, the thrust is the proportional to the square of the flux.

Fig. 12 shows the characteristic between thrust of the I-core side and air-gap length. The MMF is kept constant at 140 A. From Fig. 11, it is confirmed that the thrust is inverse proportion to the square of the air-gap length. As a reason for that the flux in the electromagnet is almost inverse proportional to the air-gap length.

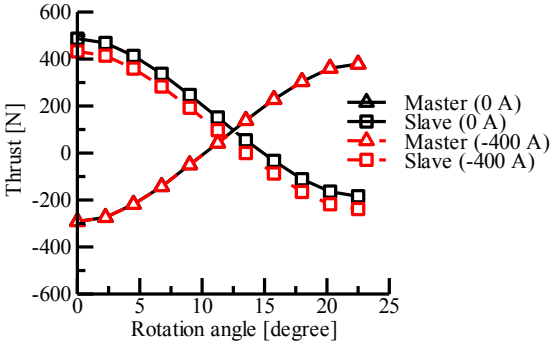

(a) Thrust at F = 0 A and 400 A. The slave side decreases the thrust by 11.1% when the MMF changes from 0A to -400 A.

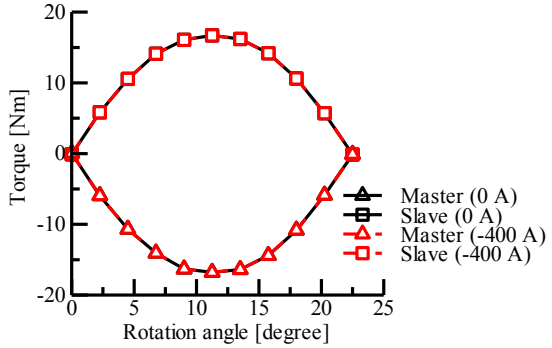

(b) Torque at F = 0 A and 400 A. the torque at F = 0 A is same as that at F = -400 A because the direction of the MMF by the electromagnet is axial direction.

Fig. 8. Analysis results of thrust and torque.

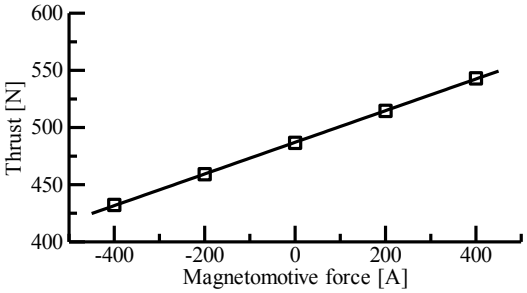

Fig. 9. Characteristic between thrust and MMF when the rotation angle is 0 degree. The change in the thrust is 111 N between F = -400 A and F = 400 A.

From Fig. 11 and 12, the analysis results agree well with the experimental results. Therefore, the validity of the thrust analysis by the FEM is confirmed.

VII. Conclusion

In this paper, the FESS (3.0-MJ, 2900-r/min) using low cost ball bearings and general purpose induction motor is evaluated. From the experimental results, the charge and discharge efficiency of the FESS is 60.7% (charge 80.7%, discharge 75.1%). Therefore, the second prototype FESS is applied to the PMSM, the SSGB and the magnetic coupling with variable thrust structure in order to achieve high efficiency and longer lifetime. The estimated charging efficiency is achieved to

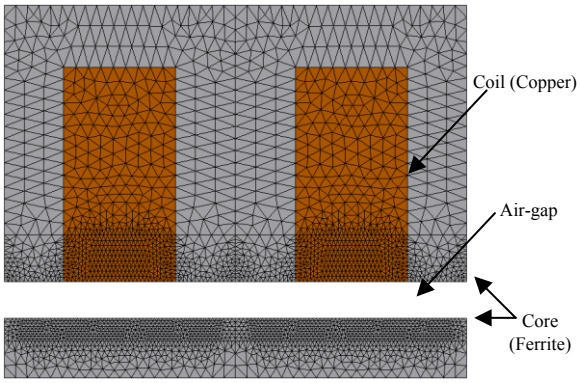

Fig. 10 Analysis model of the prototype electromagnet. The turn number of coil is 140 and the core is PC40EI60/TDK.

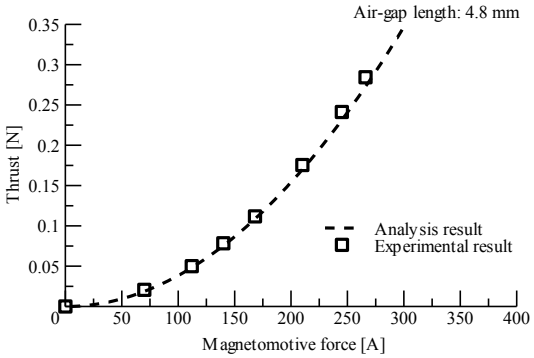

Fig. 11 Characteristic between thrust of the I-core side and MMF. The experimental result are almost same as the analysis result.

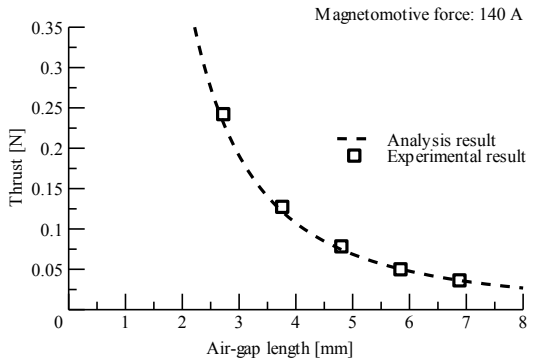

Fig. 12 Characteristic between thrust of the I-core side and air-gap length. The thrust is inverse proportion to the square of the air-gap length.

86.9% and the estimated discharging efficiency is achieved to 82.8% at the second prototype. Thus, it is expected to improve the charge and discharge efficiency by applying the PMSM and the SSGB. In addition, the thrust of the proposed magnetic coupling can be changed 11.1% by the electromagnet. Furthermore, the prototype is developed to evaluate the validity of the thrust analysis. As a result, it is confirmed that the experimental results are almost same as the analysis results.

The future work is the control of the magnetic coupling and the measurement of the charge and discharge efficiency for the second prototype FESS.

REFERENCES

[1] M.Uno and K.Tanaka, "Accelerated Charge-Discharge Cycling Test and Cycle Life Prediction Model for Supercapacitors in Alternative Battery Applications" IEEE Trans. on Industrial Electronics, Vol.60, No.6, pp.2131-2138 (2013)

[2] C. Zhang, K.J. Tseng, T.D. Nguyen, and S. Zhang, "Design and loss analysis of a high speed flywheel energy storage system based on axial-flux flywheel-rotor electric machines", IPEC-Sapporo, pp.886-891 (2010)

[3] Frank N. Werfel, Uta Floegel-Delor, Thomas Riedel, Rolf Rothfeld, Dieter Wippich, Bernd Goebel, Gerhard Reiner, and Niels Wehlau, "A Compact HTS 5 kWh/250 kW Flywheel Energy Storage System", IEEE Trans. on Applied Superconductivity, Vol.17, No.2, pp.2138-2141 (2007)

[4] M. Strasik, P. E. Johnson, A. C. Day, J. Mittleider, M. D. Higgins, J. Edwards, J. R. Schindler, K. E. McCrary, C. R. McIver, D. Carlson, J. F. Gonder, and J. R. Hull, "Design, Fabrication, and Test of a 5-kWh/100-kW Flywheel Energy Storage Utilizing a High-Temperature Superconducting Bearing", IEEE Trans. on Applied Superconductivity, Vol. 17, No.2, pp.2133-2137 (2007)

[5] B.H.Kenny, P.E.Kascak, R.Jansen, T.Dever, and W.Santiago, "Control of a High-speed Flywheel System for Energy storage in Space Applications", IEEE Trans. on Industry Applications, Vol. 41, No. 4, pp. 1029-1038 (2005)

[6] Z.Kohari, Z.Nadudvari, L.Szlama, M.Keresztesi, and I.Csaki, "Test Results of a Compact Disk-type Motor/Generator Unit With Superconducting Bearings for Flywheel Energy Storage Systems With Ultra-low Idling Losses", IEEE Trans. on Applied Superconductivity, Vol. 21, No. 3, pp. 1497-1501 (2011)

[7] K.Murakami, M.Komori, and H.Mitsuda, "Flywheel Energy Storage System Using SMB and PMB", IEEE Trans. on Applied Superconductivity, Vol. 17, No. 2, pp. 2146-2149 (2007)

[8] M. Ortuzar, J. Moreno, and J. Dixon, "Ultracapacitor-based Auxiliary Energy System for an Electric Vehicle: Implementation and Evaluation", IEEE Trans. on Industrial Electronics, Vol. 54, No. 4, pp.2147-2156 (2007)

[9] Y. Sato and A. Tamura, "Characteristics of Outwardly Pumping Spherical Spiral Groove Bearings : Part 1, Load Capacity", Bulletin of the JSME, Vol. 22, No. 174, pp.1834-1839 (1979)

[10] T. Lubin, S. Mezani, and A. Rezzoug, "Simple Analytical Expressions for the Force and Torque of Axial Magnetic Couplings", IEEE Trans. on Energy Conversion, Vol. 27, No. 2, pp.536-546 (2012)

[11] H. J. Shin, J. Y. Choi, S. M. Jang, and K. Y. Lim, "Design and Analysis of Axial Permanent Magnet Couplings Based on 3D FEM", IEEE Trans. on Magnetics, Vol. 49, No. 7, pp.3985-3988 (2013)